Computational investigation of ammonia-hydrogen peroxide blends in HCCI engine mode

Omar Shafiq⬤ and Efstathios-Al. Tingas⬤

Abstract

The potential use of hydrogen peroxide as an ignition promoter to enable the use of ammonia in compression ignition engines is explored in the current study. A simplified numerical HCCI engine model within the Chemkin Pro suite is employed. The numerical investigation reveals that the proposed use of hydrogen peroxide is significantly more advantageous against the more conventional method of preheating the intake charge to achieve ignition, whilst using a glow plug. In particular, the IMEP, power and torque exhibit an increase greater than 65% along with a spectacular decrease of NOx emissions reaching in certain cases a 9-fold decrease. The thermal efficiency exhibits a more moderate, yet non-negligible increase, around 5%. Generally, the incremental increase of hydrogen peroxide leads to the increase of the IMEP, power and torque as well as the maximum temperature and, hence, NOx emissions. These increases are largely linear with the hydrogen peroxide addition. Finally, the introduction of hydrogen peroxide leads to a two-stage ignition process, where the first ignition stage was found to be instrumental to the control of the ignition process, and, therefore, the system's efficiency. Further research is required to substantiate further the feasibility and the the limitations of the proposed technology which can enable the rapid decarbonization of heavy duty applications, such as marine ships and trucks.

Introduction

The existing climate crisis is a product of human-induced actions over the past centuries. With a rapid increase in human population and demand in various sectors, an exponential growth in greenhouse gases has been observed. The transportation sector plays a significant role in the increase of carbon emissions, with 23% of all emissions generated in Europe arising due to heavy reliance on fossil fuels used by vehicles.[1] This have motivated policy makers, particularly in the west, to introduce mandates that will phase out petrol and diesel cars in the next 10–15 years.[2–4] For instance, the UK, Sweden and the Netherlands have decided to end the sales of new petrol and diesel cars by 2030 while Norway has pledged a more ambitious plan, advancing the ban date to 2025.[5–8] An important detail to note, is that all the strict and ambitious regulations concern mainly cars, where electrification has made significant technological advancements in the last decade. Hence, electric vehicles (EVs) have been promoted by policy

makers and the industry as a viable alternative to petrol and diesel cars and the cost reduction that has been achieved at the same time, have also made EVs a potentially affordable solution.[9,10] However, electrification is far from an attractive solution for heavy duty transport applications, such as trucks and marine ships, both predominantly powered by compression ignition (CI) engines due to the requirement for high efficiency.[11,12]

As a result, the research on decarbonization technologies applicable to heavy-duty transport applications has intensified over the recent years. One of the alternative fuels that have attracted significant interest is ammonia. Ammonia is considered by many as an ideal

School of Engineering and the Built Environment, Edinburgh Napier University, Edinburgh, UK

Corresponding author:
Efstathios-Al. Tingas, Edinburgh Napier University, School of Engineering and the Built Environment, 10 Colinton Road, Edinburgh, EH10 5DT, UK.
Email: e.tingas@napier.ac.uk

candidate to replace fossil fuels in ICEs not only for propulsion but also for power generation purposes.[13–16] In principle, ammonia is a hydrogen energy carrier with one of the highest gravimetric and volumetric hydrogen densities.[14] The energy density of liquid ammonia is 15.6 MJ/l, that is, much higher than liquid hydrogen (9.1 MJ/l) and even more higher than compressed hydrogen (5.6 MJ/l at 70 MPa). This translates to a driving range of 756 km with a 60.6 l fuel tank of ammonia, which is almost twice the range provided by a liquid hydrogen tank (417 km) holding the same volume and almost three times the range yielded by a compressed hydrogen tank (254 km) again, holding the same volume.[14] When compared to hydrogen, ammonia features two additional important advantages; its storage and transportation is much easier due to an established and reliable infrastructure already being in place.[13–16] Therefore, it is not surprising that the use of ammonia in heat engines is not new and dates decades back.[17] However, one of ammonia's unique features that renders its use in heat engines extremely challenging is the very high auto-ignition temperature, more than 130 K higher than hydrogen. This favors the use of spark ignition (SI) engine mode, where ignition is initiated by a spark plug. As a result, most research on ammonia use in heat engines has been performed in the context of SI engines.[13,18–24] On the other hand, the thermodynamic conditions achieved in the engine cylinder in conventional CI engines are such that prohibit the use of ammonia. To tackle ammonia's high resistance to auto-ignition in CI engines, three strategies have been proposed.[17,25] The first is the use of high compression ratios (> 35:1).[18,26] The second is the use of a glow plug to properly preheat the charge, thereby facilitating ignition, combined with increased compression ratios.[27] The available literature on both these strategies has generally been quite scarce and practically stopped decades back because of the great difficulty in enabling a smooth engine operation as a consequence of ammonia's low reactivity, high auto-ignition temperature and low flame speed.[17,25] Ultimately, using such high compression ratios – in context of vehicular applications, is seen as impractical as it would require extensive engine modifications and also result in higher in-cylinder temperatures. Furthermore, the use of high compression ratios can lead to issues such as ringing, which occurs when the intensity of a combustion cycle is too high. This ultimately leads to an expansion of gas at dangerous speeds causing oscillation within the cylinder.[28]

An alternative and more attractive approach is the use of a more reactive fuel along with ammonia, which acts as an ignition promoter to counteract ammonia's low reactivity and low flame speed. Diesel has been by far the most popular choice to this regard, enabling the use of ammonia to as much as 95% of the fuel blend.[29,30] Other fuels that have been tested in a dual fuel CI engine mode are DME,[31,32] kerosene,[33,34] and hydrogen with proper charge preheating.[28,35,36] Of all the aforementioned fuel choices, only hydrogen is non carbon-based. But the preheating of the charge in the case of hydrogen has a detrimental effect on the engine performance characteristics.[28] Therefore, the ignition promoter should ideally be: (i) sufficiently strong to enable ignition without requiring any charge preheating, and (ii) non-carbon based, to avoid the production of any CO_2, the primary greenhouse gas.

A potential candidate to serve as an ignition promoter for ammonia's combustion in CI engines is hydrogen peroxide (H_2O_2). Hydrogen peroxide is a well-known ignition promoter which has been used since the 1930s as a propellant in aerospace and military applications.[37] In transport-related applications, it has been used alongside fuels such as diesel,[38–41] jatropha oil,[42] butanol,[43] and hydrogen.[44–46] Hydrogen peroxide has few advantages that render it a compelling candidate for use in CI engines. Firstly, it is non-carbon based and can also be produced from renewable sources.[47] Secondly, an infrastructure mechanism for its logistics support already exists, since it is a substance used in many other applications, such as for medical use as an antiseptic, domestic use as a cleanser and disinfectant, and in the food sector for processing and bleaching certain foods.

The available scientific literature on the use of ammonia and hydrogen peroxide blends is extremely scarce. Khalil et al.[48] used batch reactor simulations to demonstrate the strong effect that hydrogen peroxide can have on the ignition delay time promotion of ammonia. They showed that a 2% addition of H_2O_2 can induce a drop to the ignition delay time by a factor of 30. Using sophisticated mathematical tools from the computational singular perturbation (CSP) theory, they reported that the reaction that controls the ignition process of ammonia is $H_2O_2 \ (+M) \rightarrow 2OH \ (+M)$ (which explains the strong effect of hydrogen peroxide addition on the ignition delay time) and that ammonia ignition occurs as a thermal explosion. They also reported a negligible increase of NOx emissions as a result of the hydrogen peroxide addition. Wu and Chen[49] explored numerically the effect of hydrogen peroxide addition in ammonia/air mixtures in the context of one-dimensional premixed laminar flames and reported a substantial increase of the laminar flame speed and the adiabatic flame temperature. They also reported an increase of NO emissions as a result of the obtained flame temperatures and suggested the use of fuel lean mixtures to counteract the increased NOx emissions. Khalil et al.[50] later extended their original computational work to include steam dilution in their ammonia/hydrogen peroxide batch reactor simulations. Using CSP tools, they revealed that NOx formation is mainly due to the thermal NO mechanism, with the fuel-bound nitrogen mechanism having negligible effect on NOx production. More importantly, they highlighted that the hydrogen peroxide addition can reverse the inherent effect of steam dilution in retarding the ignition delay time, by facilitating the increased

production of OH radicals. Finally, Yang et al.[51] investigated the effect of hydrogen peroxide addition on ammonia-based counter-flow diffusion flames. Their numerical work showcased the dual role hydrogen peroxide has: that of a fuel and that of an oxidiser. They reported that increase of the hydrogen peroxide in the fuel stream above a specific percentage leads to a substantial and qualitative change of the flame structure.

All the aforementioned studies significantly increased our understanding on ammonia/hydrogen peroxide combustion. The reported promising results clearly demonstrate the necessity for further research that will showcase the feasibility of the proposed technology. Therefore, the aim of the current work is to build on the available knowledge and explore the feasibility of using ammonia/hydrogen peroxide blends in the context of a simplified HCCI engine model, in view of engine performance characteristics, combustion phasing and NOx emissions. The simplified numerical model available in the Chemkin Pro[52] suite is selected because it will allow for a wide exploration of the parametric space with a small computational cost. The employed computational model is a simplified one, therefore has some inherent weaknesses due to the underlying assumptions made to reach a simple mathematical formulation. Yet, it can still provide some valuable insight if carefully used, which justifies its wide use by the research community.[35,53,54] Subsequently, the results produced by such a simplified model will need to be treated with care, and the emphasis should be placed on exploring the qualitative aspects rather than the quantitative ones. In addition, the obtained results will be used to identify trends that can credibly inform subsequent analyses of the fuel blend in either high-fidelity simulations or real-world engine testing.

Material and methods

In the current work a single zone zero-dimensional HCCI engine model was employed, available within the Chemkin Pro suite. The employed model is fully closed (no mass exchange) and solves the species mass fractions and energy equations, along with an additional equation for the volume change. In principle, the model considers the system to be fully homogeneous, with the effect of the transport processes being negligible. Since the HCCI combustion is a chemical kinetic combustion process controlled by the thermodynamic conditions of the in-cylinder charge and not by the flame propagation these approximations are reasonable.[55] Yet, the results should be treated with care because the preparation of a fully homogeneous charge with no spatial compositional and thermal inhomogeneities may not always be used (sometimes intentionally) and in these cases mixed combustion modes (deflagration and spontaneous ignition) can co-exist, thereby affecting the overall engine performance.[56–58] For a detailed description of the

model the reader is referred to the Chemkin Pro manual.[52] Here, only a brief description will be provided.

Considering a system of Y_k mass fractions ($k = 1, ..., N$), $\dot{\omega}_k$ being the molar production rate of the k-th species and W_k the respective molecular weight, the species mass fraction governing equation can be written as:

$$\frac{dY_k}{dt} = v\dot{\omega}_k W_k \tag{1}$$

where v is the mixture's specific volume and t represents time. The energy equation can then be expressed as:

$$c_v \frac{dT}{dt} = -v \sum_{k=1}^{N} e_k \dot{\omega}_k W_k - p\frac{dv}{dt} - Q_{losses} \tag{2}$$

where c_v is the specific heat of the mixture evaluated at constant volume, e_k is the internal energy of the k-th species, p is the pressure and Q_{losses} is the net heat flux directed out of the reactor. The ideal gas equation is also used to calculate the pressure of the mixture:

$$p = \frac{\rho RT}{\tilde{W}} \tag{3}$$

where ρ is the density of the mixture, $\tilde{W}$ is the mean molecular weight of the mixture and R is the universal gas constant. In equation (2) the rate of change of the specific volume is given by:

$$\frac{dv}{dt} = \frac{1}{m}\frac{dV}{dt} \tag{4}$$

where m is the total mass of the mixture and V is the volume of the system given by the following equation:

$$\frac{V}{V_c} = 1 + \frac{C-1}{2}\left[R + 1 - cos\theta + \sqrt{R^2 - sin^2\theta}\right] \tag{5}$$

where V_c is the clearance volume, C is the compression ratio, and θ is the crank angle. Then, the volume rate of change can be calculated by:

$$\frac{d(V/V_c)}{dt} = \Omega\left(\frac{C-1}{2}\right)sin\theta\left[1 + \frac{cos\theta}{\sqrt{R^2 - sin^2\theta}}\right] \tag{6}$$

where Ω is the rotation rate of the crank arm. In the case of adiabatic conditions, Q_{losses} in equation (2) becomes zero. Otherwise, Q_{losses} can be computed by the equation:

$$Q = hA(T - T_{wall}) \tag{7}$$

where h is the heat transfer coefficient, A is the internal surface area of the cylinder, T is the temperature of the gas, and T_{wall} is the wall temperature, maintained at 430 K. The heat transfer coefficient h, can be calculated from equation (8):

$$h = \lambda \alpha Re^b Pr^c D^{-1} \tag{8}$$

Table 1. Engine parameters and operating conditions.

Compression ratio	17
Bore	100 mm
Stroke	105 mm
Engine speed	750, 1150 rpm
Connecting rod to crank radius ratio	3.714286
Intake temperature	320 K
Intake pressure	1.065 atm

where λ is the gas conductivity, Re and Pr are the Reynolds and Prandtl numbers, respectively, and α, b, and c were constants that were assigned the default values of 0.035, 0.71 and 0, respectively. The velocity in Reynolds number was calculated on the basis of the average gas velocity, given by the Woschni correlation. In the latter, the modeling parameters C_{11}, C_{12}, and C_2 were given their default values of 2.28, 0.308, and 3.24, respectively.

The chemistry in the simulations was modeled by the detailed chemical kinetic mechanism of Zhang et al.[59] which includes 38 species and 262 chemical reactions and has been extensively validated.[59] The engine's parameters are summarized in Table 1. In all simulations, the compression ratio was maintained at 17:1, whilst the bore and stroke were 100 and 105 mm, respectively. Unless otherwise stated, the intake temperature and pressure remained constant at 320 K and 1.065 atm. Since hydrogen peroxide is in liquid phase at these conditions, a fuel vaporizer would need to be used, like those typically used for diesel operation in HCCI mode.[60–62] The study focused on two engine speeds, 750 and 1150 rpm. Finally, all simulations started at −180 crank angle degrees after top dead center (CAD aTDC) and ended at +180 CAD aTDC.

Addition of H_2O_2 was done on a mole fraction basis of NH_3. For example, a 10% addition of H_2O_2 specifies the mole fraction of H_2O_2 added on a 10% basis of the mole fraction of NH_3. However, as a result of hydrogen peroxide acting as an oxidiser (and a fuel), the traditional method of calculating the equivalence ratio: $\varphi = (F/A)/(F/A)_{stoic}$ cannot be implemented and therefore an alternative method, where the equivalence ratio was denoted as the effective equivalence ratio (φ_{eff}), similar to the approach taken by Tingas[45,46] and Hui et al.[63] in their investigations was employed:

$$\varphi_{eff} = \frac{(X_{NH_3}/(0.5X_{H_2O_2} + X_{O_2})}{(X_{NH_3}/X_{O_2})_{stoic}} \quad (9)$$

Equation (9) is derived on the assumption that 1 mol of H_2O_2 generates 1 mol of H_2O and 0.5 mol of O_2. The notation *stoic* indicates that stoichiometric conditions must be considered. Indicative values of the initial mole fractions used for the examined compositions are shown in Table 2.

On the basis of the indicated work being W_{ind}, and the engine speed denoted by N, the indicated power can be defined as:

$$P_{ind} = \frac{W_{ind}N}{2} \quad (10)$$

Subsequently, torque can be derived using

$$T = \frac{P_{ind}}{2\pi N} \quad (11)$$

whilst the swept volume (V_{disp}) can be used to define the indicated mean effective pressure,

$$IMEP = \frac{W_{ind}}{V_{disp}} \quad (12)$$

using $V_{disp} = (\pi/2)D^2L_A$, where D denotes the bore diameter and $L_A = 36.8$ mm, the crank arm radius. Finally, the thermal efficiency is given as

$$n_{th} = \frac{1}{sfc \cdot Q_{HV}} \quad (13)$$

where sfc indicates the specific fuel consumption ($sfc = (m_fN)/(2P_{ind})$), m_f the fuel mass and Q_{HV} indicates the heating value of the fuel.

Results and discussion

Comparison of the hydrogen peroxide use strategy against the glow plug approach

The first part of the investigation is focused on comparing the proposed technology (i.e. the use of hydrogen peroxide as an ignition promoter) against the more conventional use of a glow plug which preheats sufficiently the charge to enable its ignition close to the TDC. We firstly consider adiabatic conditions (i.e. Q_{losses} in equation (2) is zero), at $\varphi_{eff} = 0.3$, 0.4, and 0.5. To allow a fair and meaningful comparison between the two strategies we keep the ignition CAD (CAD_{ign}) constant at 12.6 and 17.5 CAD aTDC for $\varphi_{eff} = 0.3$ and 0.4/0.5, respectively. The results of this analysis are displayed in Table 3. For example, at 750 rpm and $\varphi_{eff} = 0.3$, we would need to add 24% H_2O_2 to achieve $CAD_{ign} = 12.6$ CAD aTDC. With the glow plug strategy (and in the absence of any H_2O_2), we would need to increase the inlet temperature by 141.57 K, to $T_{in} = 461.57$ K, so as to achieve the same $CAD_{ign} = 12.6$ CAD aTDC. It is noted that CADign is determined on the basis of the maximum temperature rate of change.

In particular, the results at an effective equivalence ratio of $\varphi_{eff} = 0.3$ and an engine speed of 750 rpm, highlight a significant increase of 69% and 67% in IMEP and power/torque, respectively, as a result of the addition of hydrogen peroxide. In the absence of any hydrogen peroxide the inlet temperature would need to be increased by 44%, from 320 to 461.57 K. The hydrogen peroxide addition also leads to a small increase of the thermal efficiency (4%) and a notable decrease (11%) of the maximum temperature. The latter is simply the result of the much lower inlet temperature used (320 K) which is 31% lower than the one used with the glow plug approach. The notable decrease of the maximum temperature is important because as was reported

Table 2. Indicative values of the initial mole fraction values of the charge at various equivalence ratios.

ϕ_{eff}	% H_2O_2	X_{NH_3}	$X_{H_2O_2}$	X_{O_2}	X_{N_2}
0.2	0	0.053030	0.000000	0.198864	0.748106
0.2	1	0.053069	0.000531	0.198744	0.747656
0.2	5	0.053225	0.002661	0.198264	0.745849
0.2	10	0.053422	0.005342	0.197660	0.743576
0.2	20	0.053819	0.010764	0.196438	0.738980
0.2	30	0.054222	0.016266	0.195198	0.734314
0.2	35	0.054425	0.019049	0.194571	0.731955
0.3	0	0.077491	0.000000	0.193727	0.728782
0.3	1	0.077574	0.000776	0.193547	0.728104
0.3	5	0.077908	0.003895	0.192822	0.725375
0.3	10	0.078329	0.007833	0.191906	0.721932
0.3	20	0.079186	0.015837	0.190045	0.714932
0.3	30	0.080061	0.024018	0.188144	0.707777
0.3	35	0.080506	0.028177	0.187177	0.704140
0.4	0	0.100720	0.000000	0.188849	0.710431
0.4	1	0.100860	0.001009	0.188608	0.709524
0.4	5	0.101425	0.005071	0.187636	0.705868
0.4	10	0.102140	0.010214	0.186406	0.701240
0.4	20	0.103601	0.020720	0.183893	0.691786
0.4	30	0.105105	0.031532	0.181306	0.682057
0.4	35	0.105874	0.037056	0.179985	0.677086

in the earlier work of Khalil et al.[50] the NO production largely depends on the thermal NO mechanism. This justifies the significant decrease of NOx production displayed in Table 3, where it is shown that the addition of hydrogen peroxide leads to a 52% decrease in NOx. The only caveat with the hydrogen peroxide addition is the increase of the maximum pressure by 30%. However, this pressure increase is accompanied by a 85% increase of the rapid burning angle (RBA), which would mitigate any knock occurrence. It is noted that the RBA is defined as the difference between CAD90 and CAD10, that is, the crank angle between 10% and 90% of the heat release rate.

Increasing the engine speed from 750 to 1150 rpm while maintaining the effective equivalence ratio and the CAD_{ign} constant at 0.3 and 12.6 CAD aTDC, respectively, requires the increase of the hydrogen peroxide addition from 24% to 29.5%. To achieve the same CAD_{ign} in the absence of any hydrogen peroxide we would need to increase the inlet temperature from 320 to 475.68 K, that is, a 49% increase. Hence, we observe that by increasing the engine speed from 750 to 1150 rpm the required increase of the inlet temperature in the absence of any hydrogen peroxide is 5% higher, while hydrogen peroxide needs to be increased by 5.5% (from 24% to 29.5%). At 1150 rpm, hydrogen peroxide addition leads to a more pronounced increase of the IMEP, torque and power; IMEP increases by 76% (69% at 750 rpm) while power and torque both increase by 77% (67% at 750 rpm). On the other hand, the increase induced to the thermal efficiency due to hydrogen peroxide addition is maintained the same at 4%. The same applies for the decrease of the maximum temperature (11% decrease) and NOx emissions. However, the adverse effect on the maximum pressure becomes more intense, since hydrogen peroxide now leads to a 33% increase of the maximum pressure (as compared to a 30% increase at 750 rpm), and the RBA increase is limited to a 45% increase (down from an 85% increase at 750 rpm).

Moving onto $\varphi_{eff} = 0.4$, similar trends can be noted as a result of the hydrogen peroxide addition, when compared to that of $\varphi_{eff} = 0.3$. Firstly, the inlet temperature has to be increased by 46% and 50% in the absence of any hydrogen peroxide for 750 and 1150 rpm, respectively. These values are larger when compared to the 44% and 49% increases required at $\varphi_{eff} = 0.3$ (for 750 and 1150 rpm, respectively). The increase seen in IMEP, power/torque and thermal efficiency due to the hydrogen peroxide addition are

Table 3. Engine performance results for different engine speeds (750 and 1150 rpm) and effective equivalence ratios (φ_{eff} = 0.3, 0.4, 0.5) with and without H_2O_2 content. Each case of NH_3 + H_2O_2 has a respective case of pure ammonia which is preheated. All cases with H_2O_2 content have a constant intake temperature of 320 K. CAD_{ign} is maintained constant at 17.5 aTDC, whilst the only exception being the results obtained at φ_{eff} = 0.3, where CAD_{ign} = 12.6 aTDC.

Speed (rpm)	φ_{eff}	%H_2O_2	T_{in} (K)	CAD_{ign} (CAD aTDC)	RBA (CAD aTDC)	IMEP (bar)	Power (J/sec)	Torque (N m)	n_{th}	T_{max} (K)	NOx (ppm)	P_{max} (bar)
750	0.3	24.00	320.0	12.6	14.8	7.1	3640.0	46.3	66.6	1740.1	2106.5	82.1
		0.00	461.6	12.6	8.01	4.2	2177.8	27.7	64.3	1947.9	4359.1	63.3
	0.4	19.58	320.0	17.5	17.8	8.7	4460.9	56.8	63.7	1903.9	3462.8	76.8
		0.00	465.7	17.5	10.2	5.2	2657.4	33.8	60.9	2097.6	6484.8	57.6
	0.5	17.84	320.0	17.5	15.4	10.2	5280.2	67.2	62.0	2102.9	5893.5	85.6
		0.00	471.8	17.5	8.7	6.1	3125.2	39.8	59.5	2283.2	9337.5	62.1
1150	0.3	29.50	320.0	12.6	12.0	7.2	5716.3	47.5	66.6	1750.4	2220.9	82.6
		0.00	475.7	12.6	8.3	4.1	3228.9	26.8	64.1	1970.3	5338.3	62.1
	0.4	24.61	320.0	17.5	13.9	8.8	6991.5	58.1	63.5	1917.9	3684.3	77.5
		0.00	479.5	17.5	10.5	5.0	3948.2	32.8	60.8	2117.5	6897.1	56.5
	0.5	28.00	320.0	17.5	9.1	10.6	8369.3	69.5	60.8	2155.1	6915.3	88.3
		0.00	485.6	17.5	7.0	5.9	4644.6	38.6	59.4	2301.4	9779.8	61.0

maintained and remain practically unchanged when increasing φ_{eff} from 0.3 to 0.4, at both engine speeds (750 and 1150 rpm): IMEP increases by 67% and 76% (compared to 69% and 76% at $\varphi_{eff} = 0.3$), power/torque increase by 68% and 77% (compared to 67% and 77% at $\varphi_{eff} = 0.3$), thermal efficiency increases by 5% and 4% (compared to 4% at $\varphi_{eff} = 0.3$). On the other hand, some more noticeable changes in the trends for the other variables are noted. The decrease of the maximum temperature due to the hydrogen peroxide addition becomes less pronounced at $\varphi_{eff} = 0.4$, reaching a 9% decrease in both speeds (compared to 11% at $\varphi_{eff} = 0.3$). This has a direct effect on the NOx emissions, which now decrease at a lower magnitude, by 47% (compared to 52% at $\varphi_{eff} = 0.3$). In addition, the increase of the maximum pressure becomes more pronounced reaching 33% and 37% at 750 and 1150 rpm, respectively, (compared to 30% and 33% at $\varphi_{eff} = 0.3$). Finally, the RBA becomes less favored by the addition of hydrogen peroxide, exhibiting 75% and 32% increases at 750 and 1150 rpm, respectively, (compared to 85% and 45% at $\varphi_{eff} = 0.3$).

At $\varphi_{eff} = 0.5$ the required temperature increase in the absence of hydrogen peroxide becomes more pronounced, reaching 471.75 and 485.62 K for 750 and 1150 rpm, respectively. These values represent 47% and 52% increases compared to the cases where hydrogen peroxide addition is considered, where the inlet temperature is maintained at 320 K. In addition, the increase of IMEP, power and torque due to the addition of hydrogen peroxide is maintained significantly high at both speeds: IMEP increases by 67% and 80% while power/torque increase by 69% and 80%, at 750 and 1150 rpm, respectively. The thermal efficiency still experiences a small increase due to the addition of hydrogen peroxide, with the higher speed being even less favored (4% and 2% increase at 750 and 1150 rpm, respectively). Moreover, hydrogen peroxide addition still induces a decrease of the maximum temperature affecting negatively the production of NOx but both decreases become less pronounced at both engine speeds; T_{max} decreases by 8% and 6%, while NOx reduces by 37% and 29% at 750 and 1150 rpm, respectively. Finally, the maximum pressure increases by 38% and 47% at 750 and 1150 rpm, respectively, due to the addition of hydrogen peroxide.

In summary, the following conclusions can be drawn for the hydrogen peroxide addition approach when compared to the inlet preheating method:

- IMEP, power and torque all increase significantly ($>65\%$), with their increases remaining practically unaffected by the increase of the effective equivalence ratio but becoming more pronounced at higher engine speeds. This will be discussed further in the following chapters.
- the thermal efficiency exhibits a small increase, regardless the effective equivalence ratio and the engine speed.

- the maximum temperature is notably decreased by 6%–11%. This decrease has a significant effect on the production of NOx, leading to a decrease of 29%−52%. The decreases of T_{max} and NOx both become less pronounced as the effective equivalence ratio increases.
- the maximum pressure increases significantly by 30%–45%. Its increase is favored by the increase of the effective equivalence ratio and/or the increase of the engine speed.
- the RBA increases significantly by 30%−85%, with its increase becoming less pronounced as the effective equivalence ratio and/or the engine speed increase.

In order to understand what causes the higher engine performance with the use of hydrogen peroxide, we have to remember that the introduction of hydrogen peroxide leads to the increase of the mixture's energy density. Considering that the introduction of hydrogen peroxide occurs on a volumetric basis and that hydrogen peroxide has significantly higher volumetric energy density than ammonia at the examined conditions (4.428 MJ/l for H_2O_2[64] against 1.116 MJ/l for ammonia[65] at 320 K and 1 bar), it is reasonable to expect that the mixture of NH_3/H_2O_2 will be more energy dense. The higher energy density favors the higher pressure reached, as shown in Figure 1, which in turn increases the indicated work, and hence IMEP, power and torque.

It is worth noting that for the cases considered in Table 3, the inlet temperature in the absence of any hydrogen peroxide had to be increased by 44%–52%. At the same time, the hydrogen peroxide approach required hydrogen peroxide addition ranging between 24% and 28%. A closer investigation of the inlet temperature and hydrogen peroxide addition values reveals something unexpected. In the cases where no hydrogen peroxide is added to the mixture, the inlet temperature has to be increased with the increase of the equivalence ratio. This is not surprising since the reactivity of ammonia decreases as the mixture becomes richer, that is, the ignition delay time increases when moving from fuel lean to stoichiometric mixtures.[66–68] The unexpected finding is the variation of the required amount of hydrogen peroxide at 1150 rpm; from fuel lean to fuel rich conditions, the required percentage of hydrogen peroxide initially decreases and then increases. This anomaly is observed at 1150 rpm and not 750 rpm where the hydrogen peroxide percentage decreases with the increase of the effective equivalence ratio.
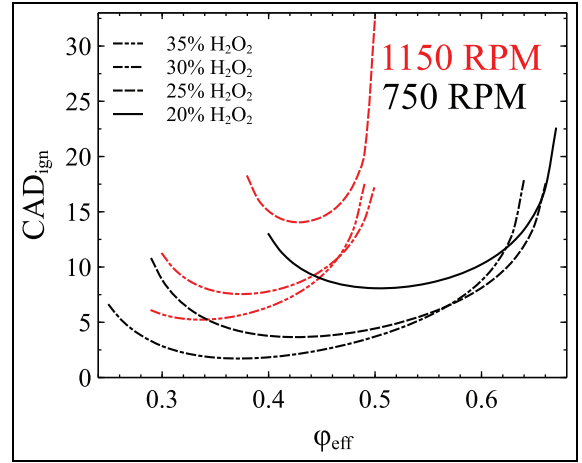
In order to investigate further this unexpected finding, in Figure 2 we present the variation of CAD_{ign} as a function of φ_{eff} for selected cases of H_2O_2 content at both engine speeds: 20%, 25%, and 30% at 750 rpm and 25%, 30%, and 35% at 1150 rpm. It is shown that in both engine speeds and all hydrogen peroxide percentages, CAD_{ign} exhibits a non-monotonic response to the increase of φ_{eff}, initially decreasing up to some
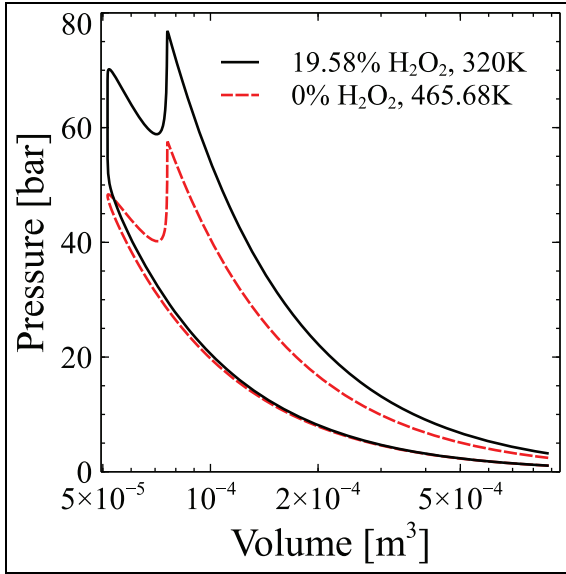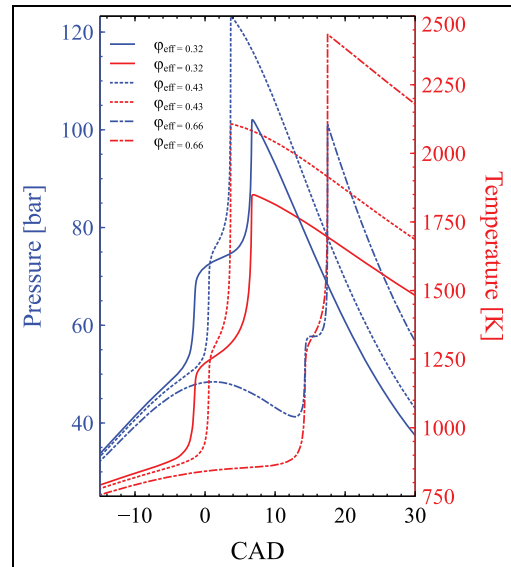
Figure 1. The P-V diagram for the cases of 19.58% H_2O_2, 320 K (solid-black line) and 0.0% H_2O_2, 465.68 K (dashed-red line), both at 750 rpm and $\varphi_{eff} = 0.4$. For further details on the two examined cases, the reader is referred to Table 3.

Figure 2. The variation of CAD_{ign} (CAD aTDC) as a function of φ_{eff} for selected cases of H_2O_2 content at 750 (black font) and 1150 (red font) rpm.

Figure 3. The evolution of pressure (bar) and temperature (K) against CAD for three cases of φ_{eff} (0.32, 0.43, 0.66) with the same hydrogen peroxide percentage (25%) and the same engine speed (750 rpm). The case of $\varphi_{eff} = 0.32$ is in the range where CAD_{ign} decreases with the increase of φ_{eff}, $\varphi_{eff} = 0.43$ represents the case with the minimum CAD_{ign} (increasing or decreasing φ_{eff} will lead to the increase of CAD_{ign}) and $\varphi_{eff} = 0.66$ is in the range where CAD_{ign} increases with the increase of φ_{eff}.

point before it starts increasing. The upper φ_{eff} limit, that is, the largest φ_{eff} value that ignition can be achieved, appears to be largely insensitive to the hydrogen peroxide content, placed at $\varphi_{eff} \approx 0.65$ and 0.5 at 750 and 1150 rpm, respectively. Therefore, unlike what was revealed in Table 3, Figure 2 highlights that the non-monotonicity in the response of CAD_{ign} as a function of φ_{eff} does not occur only at 1150 rpm but also at 750 rpm. In fact, at 750 rpm it becomes more pronounced.

In order to understand what causes the non-monotonic response in CAD_{ign}, Figure 3 displays the variation of the pressure and temperature as a function of CAD for three cases with different φ_{eff} (0.32, 0.43, 0.66) but with the same hydrogen peroxide percentage (25%) and the same engine speed (750 rpm). In essence, these cases represent three cases from those displayed in Figure 2 with the red dashed line; the case of $\varphi_{eff} = 0.32$ represents a case in the range of φ_{eff} where CAD_{ign} decreases with the increase of φ_{eff}, $\varphi_{eff} = 0.43$ represents the case where the minimum CAD_{ign} is reached and $\varphi_{eff} = 0.66$ represents one case in the φ_{eff} range where CAD_{ign} increases with the increase of φ_{eff}. Figure 3 reveals that although CAD_{ign} has a non-monotonic response among these three cases (from $\varphi_{eff} = 0.32$ to 0.43 it decreases and from $\varphi_{eff} = 0.43$ to 0.66 it increases), the first stage ignition has a monotonic response, being retarded with the increase of φ_{eff}. Notice also that for the case of $\varphi_{eff} = 0.43$ that represents the case with the minimum CAD_{ign}, the first stage ignition occurs at the TDC, that is, 0 CAD. These results indicate then that the non-monotonic response of CAD_{ign} observed in Figure 2 is due to the CAD of the first-stage ignition.

To substantiate further the critical role of the first stage ignition on the non-monotonic response of CAD_{ign} to φ_{eff}, Figure 4 displays the variation of CAD_{ign} and CAD10 against φ_{eff} for 25% H_2O_2 content at 750 rpm. CAD10 is used as a marker representative of the first ignition stage. It is clearly shown that as long as CAD10 is negative (i.e. bTDC), CAD_{ign} decreases with the increase of φ_{eff}. This is reasonable since the combustion process is favored by the thermodynamic

changes induced by the compression of the volume. As soon as the CAD10 becomes positive (i.e. aTDC) the increase of φ_{eff} leads to the increase of CAD_{ign}. Positive CAD10 suggests that the chemical system has to work against the unfavorable thermodynamic conditions produced by the volume expansion in order to reach ignition. Ammonia's very poor reactivity makes the system strongly dependent on the thermodynamic conditions produced by the piston movement close to the TDC. It is noted that the two-stage ignition exhibited herein is a feature introduced due to the addition of hydrogen peroxide as ammonia as a sole fuel exhibits single stage ignition.[50,51] Consequently, the first stage ignition is instrumental to the control of the whole ignition process as it can lead to qualitatively different outcomes.

The effect of the incremental increase of the initial amount of hydrogen peroxide on the engine performance characteristics at constant equivalence ration (ϕ_{eff})

The next analysis takes into consideration the incremental addition of H2O2 at $\varphi_{eff} = 0.2$, 0.3, and 0.4 and engine speeds of 750 and 1150 rpm and considers the effect produced on the various engine performance characteristics. The results of this numerical campaign are displayed in Figures 5 to 8.

In Figure 5(a) it is shown that the addition of hydrogen peroxide initially has a strong effect on the CAD50 advancement but shortly afterward levels off. For instance, at $\varphi_{eff} = 0.3$, ignition is first achieved with 23.5% H_2O_2 addition, incurring CAD50 equal to 11.2 CAD aTDC. Increasing the hydrogen addition by 8% further to 31.5%, CAD50 reaches 0.8 CAD aTDC, that is more than 10 degrees additional advancement. Further increase of the H_2O_2 addition to 50% incurs merely 2% further advancement of CAD50. The phenomenon of the rapid advancement of CAD50 followed by a level-off becomes more pronounced as φ_{eff} increases. On the other hand, as φ_{eff} increases the advancement of CAD50 due to the hydrogen peroxide addition occurs at higher degrees. For instance at $\varphi_{eff} = 0.3$ the incremental H_2O_2 addition leads at some point (H_2O_2 addition larger or equal to 34%) to negative CAD, that is, bTDC. However, when the effective equivalence ratio is increased to $\varphi = 0.4$, the hydrogen peroxide addition does not induce negative CAD50, regardless the percentage addition. In fact, in the case of $\varphi_{eff} = 0.4$, CAD50 never levels off as a function of H_2O_2 addition, but following a steep decrease it reaches a minimum value and then starts gradually increasing. This non-monotonic response is occurring because the first stage ignition CAD is retarded and turns from negative (i.e. bTDC) to positive (i.e. aTDC), due to the addition of H_2O_2, similar to what was described for Figures 2 to 4. The retarding of the first stage ignition due to the addition of H_2O_2 occurs for all φ_{eff} but in
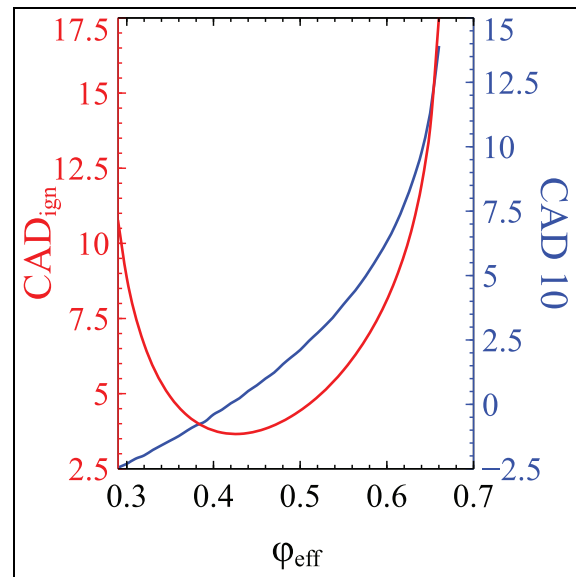

Figure 4. The variation of CAD_{ign} and CAD10 (CAD aTDC) as a function of φ_{eff} for 25% H_2O_2 content at 750 rpm.

the other two cases ($\varphi_{eff} = 0.2$ and 0.3) it never changes sign (i.e. from negative to positive), which explains why they don't exhibit the same non-monotonic response in CAD50.

As the engine speed increases, it becomes more difficult for the system to reach negative CAD50 values. In fact, the advancement of CAD50 to negative degrees is barely achieved for extremely lean mixtures of $\varphi_{eff} = 0.2$. Another significant difference between $\varphi_{eff} = 0.2$ and the other two effective equivalence ratio values is that the minimum required H_2O_2 addition to achieve ignition is significantly higher for the first. In particular, at $\varphi_{eff} = 0.2$ the minimum required H_2O_2 addition is 32.5% and 39% for 750 and 1150 rpm, respectively, while at $\varphi_{eff} = 0.3/0.4$ the respective H_2O_2 percentages are 23.5%/19.5% and 28.5%/24.5% for 750 and 1150 rpm, respectively. This is roughly a 10% difference of the minimum required H_2O_2 addition between $\varphi_{eff} = 0.2$ and 0.3/0.4. Finally, the non-monotonic response of CAD50 in the case of $\varphi_{eff} = 0.4$ becomes more pronounced.

The significant influence of the H_2O_2 addition on the combustion phasing is also reflected on the RBA, that is, the difference between CAD90 and CAD10. Figure 5(b) show that regardless the φ_{eff} and the engine speed, the addition of H_2O_2 incurs initially a dramatic drop to the RBA but after some point it levels off, similar to what was reported previously for CAD50 with the only difference being that this response occurs for all three φ_{eff} values. Yet, as φ_{eff} increases, the logarithmic response (in fact, 1/logx) of the RBA becomes more pronounced. In fact, 80% of the maximum possible decrease of the RBA (the latter occurring for 50% H_2O_2 addition) can be achieved with 40%/31%/25% H_2O_2 addition, at $\varphi_{eff} = 0.2$, 0.3, 0.4, respectively,
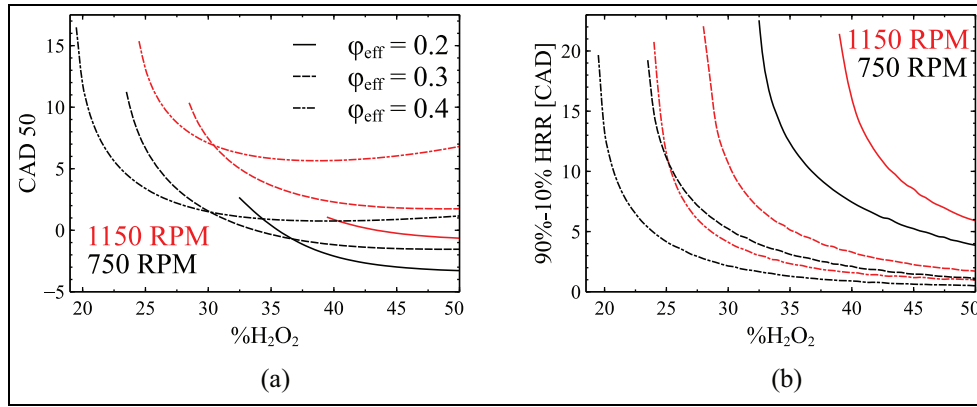
Figure 5. Variation of CAD50 (a) and the RBA (b) as a function of H_2O_2 addition for three different cases of φ_{eff} = 0.2, 0.3, 0.4 (solid, dashed, and dot dashed lines, respectively) and two different engine speeds, 750 (black font) and 1150 rpm (red font).
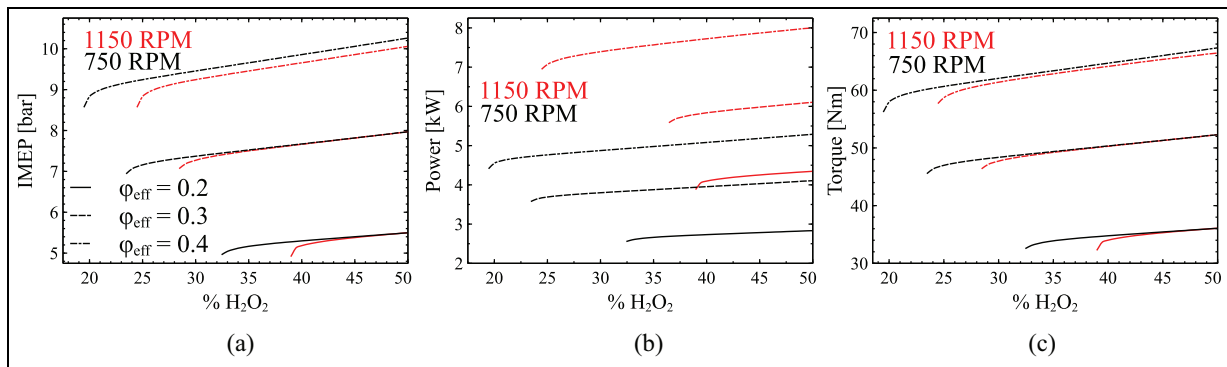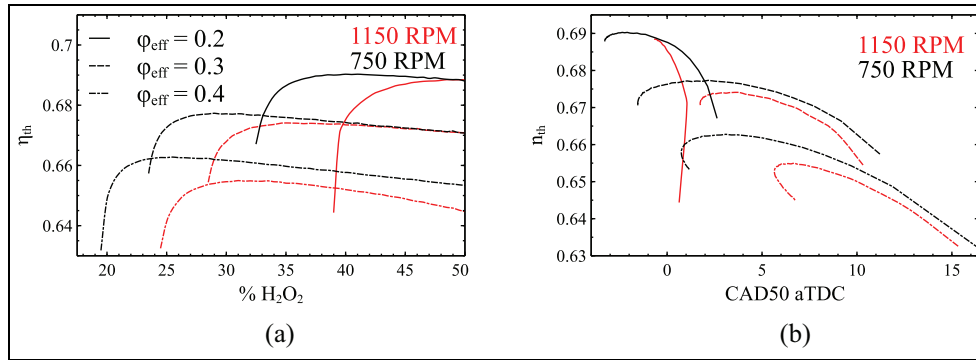

Figure 6. Variation of IMEP (a), power (b), and torque (c) as a function of H_2O_2 addition for three different cases of φ_{eff} = 0.2, 0.3, 0.4 (solid, dashed, and dot dashed lines) and two different engine speeds, 750 (black font) and 1150 rpm (red font).

when the engine speed is 750 rpm. These H_2O_2 addition percentages represent 7.5%, 7.5%, and 5.5% increases compared to the minimum required hydrogen peroxide addition contents (32.5%, 23.5%, and 19.5%) to achieve ignition of the system, at φ_{eff} = 0.2, 0.3, and 0.4, respectively. The dramatic decrease of the RBA is due to not only the advancement of CAD90 but also the retarding of CAD10 (which is correlated with the first stage ignition), as previously described.

The analysis will now focus on the effect of incremental hydrogen peroxide addition on IMEP, power and torque, as illustrated in Figure 6. Firstly, it can be easily observed that all three performance outputs exhibit in principle a linear response to the hydrogen peroxide addition. Exploiting this feature, a linear regression analysis was performed to determine how the response of IMEP, torque and power is affected by the change in φ_{eff} and engine speed. In all cases discussed next, the coefficient of determination (R^2) was always higher than 0.97. At 750 rpm it was found that gradients of the best fit lines were 2.342, 3.225, 4.367 for φ_{eff} = 0.2, 0.3, and 0.4, respectively. These results indicate that hydrogen peroxide tends to increase IMEP, power and torque and this tendency is favored as the effective

equivalence ratio increases. This finding is confirmed at the higher engine speed of 1150 rpm, where the gradients of the best fit lines were 3.124, 3.518, 4.362 for φ_{eff} = 0.2, 0.3, and 0.4, respectively. Hence, as the engine speed increases at the same φ_{eff}, the response of IMEP, power and torque tend to get characterized by a steeper gradient but this phenomenon becomes attenuated as the effective equivalence ratio increases.

Figure 6 also shows that at 750 rpm and 35% H_2O_2: (i) at φ_{eff} = 0.2, the IMEP equals to 5.2 bar, P_{ind} becomes 2.66 kW and Torque reaches 33.9 Nm; (ii) at φ_{eff} = 0.3, the IMEP is 7.5 bar, P_{ind} is 3.88 kW and Torque is 49.4 Nm; (iii) at φ_{eff} = 0.4, the IMEP becomes 9.7 bar, P_{ind} equals 4976.8 W and Torque is 63.4 Nm. These results clearly demonstrate the tremendous increase in engine performance characteristics as a richer fuel mixture is employed, yet at extremely lean conditions. It is also worth noting that at 750 rpm: (i) at ϕ_{eff} = 0.2, IMEP ranges between 5.0 and 5.5 bar, P_{ind} between 2.56 and 2.83 kW and torque between 32.6 and 36 Nm; (ii) at φ_{eff} = 0.3, IMEP ranges between 6.9 and 8.0 bar, P_{ind} between 3.58 and 4.11 kW and torque amidst 45.6–52.3 Nm; (iii) at φ_{eff} = 0.4, IMEP is between 8.6 and 10.3 bar, P_{ind} between 4.42

Figure 7. Variation of the thermal efficiency as a function of H_2O_2 addition (a) and CAD50 (b) for three different cases of $\varphi_{eff} = 0.2, 0.3, 0.4$ (solid, dashed, and dot dashed lines) and two different engine speeds 750 (black font) and 1150 rpm (red font).

and 5.29 kW and torque between 56.3 and 67.3 Nm. Hence, the highest possible increase to IMEP, power and torque in the examined range of hydrogen peroxide addition (igniting) cases rises from ∼10% at $\varphi_{eff} = 0.2$, to ∼15% at $\varphi_{eff} = 0.3$ and ∼20% at $\varphi_{eff} = 0.4$. Similarly, at 1150 rpm: (i) at $\varphi_{eff} = 0.2$, $5.1 \leqslant$ IMEP $\leqslant 5.5$ bar, $4.06 \leqslant P_{ind} \leqslant 4.35$ kW, $33.7 \leqslant$ Torque $\leqslant 36.1$ Nm; (ii) at $\varphi_{eff} = 0.3$, $7.1 \leqslant$ IMEP $\leqslant 8.0$ bar, $5.59 \leqslant P_{ind} \leqslant 6.30$ kW, $46.5 \leqslant$ Torque $\leqslant 52.3$ Nm; (iii) at $\varphi_{eff} = 0.4$, $8.8 \leqslant$ IMEP $\leqslant 10.1$ bar, $6.96 \leqslant P_{ind} \leqslant 8.00$ kW, $57.8 \leqslant$ Torque $\leqslant 66.4$ Nm. Hence, the highest possible increase to IMEP, power and torque in the examined hydrogen peroxide addition cases now becomes ∼7% at $\varphi_{eff} = 0.2$, ∼12% at $\varphi_{eff} = 0.3$, and ∼15% at $\varphi_{eff} = 0.4$, that is, decrease compared to the lower engine speed cases. Another interesting observation that can be made is that the range of values of IMEP and torque remain largely unaffected by the engine speed as opposed to the indicated power that exhibits significant increase as the engine speed, which is reasonable since it is proportional to the engine speed, as it was shown in equation (10).

The effect of H_2O_2 addition on the thermal efficiency is also displayed in Figure 7. The first observation that can be made is that the thermal efficiency generally drops with the increase of φ_{eff}. As the φ_{eff} increases, for the same % of H_2O_2 addition, the *sfc* and *QHV* both increase, which leads to the decrease of the thermal efficiency. Secondly, the incremental addition of hydrogen peroxide leads initially to a rapid increase of the thermal efficiency which at some point reaches a maximum value. Further increase of the hydrogen peroxide addition leads to a gradual decrease of the thermal efficiency. The non-monotonic response of the thermal efficiency to the addition of H_2O_2 is the net outcome of the competitive action between the *sfc* and *QHV*; the first monotonically increasing and the latter monotonically decreasing with the increase of H_2O_2. The condition where the maximum thermal efficiency is reached is when the rate of the increase of the first becomes larger than the rate of the increase of the latter. At 750 rpm, the system reaches maximum thermal efficiencies of 69.03% (40.5% H_2O_2), 67.7% (29% H_2O_2), and 66.3% (25.5% H_2O_2) thermal efficiency for

$\varphi_{eff} = 0.2, 0.3$, and 0.4, respectively. These values indicate that as the mixture becomes richer the maximum thermal efficiency is obtained for lower hydrogen peroxide percentage additions. This is in agreement with the results at 1150 rpm, where the system reaches highest thermal efficiency 68.8% (48.5% H_2O_2), 67.4% (35% H_2O_2) and 65.5% (25.5% H_2O_2) at $\varphi_{eff} = 0.2$, 0.3, and 0.4, respectively. Notice though that as the engine speed increases, the leaner the mixture the more hydrogen peroxide is required to reach the highest thermal efficiency.

To obtain further insight on the relation between the thermal efficiency and the combustion process, in Figure 7(b) the thermal efficiency is plotted against CAD50. The percentage of the added H_2O_2 increases from left to right, that is, from high to low CAD50 values. The maximum thermal efficiency is achieved in all cases when CAD50 is close to the TDC ($-2.2/-0.6$, 2.2/3.6, 3.1/6.7 for $\varphi_{eff} = 0.2, 0.3, 0.4$ at 750/1150 rpm, respectively), which is reasonable since it ensures maximum indicated work. However, as the mixture becomes leaner the CAD50 associated with the maximum thermal efficiency is advanced and in the case of $\varphi_{eff} = 0.2$ it even becomes negative. Additionally, as the engine speed increases, the CAD50 values that produce the maximum thermal efficiencies are retarded and this phenomenon becomes more pronounced as φ_{eff} increases, that is, the mixture becomes richer. Finally, notice that the non-monotonic response that is observed for $\varphi_{eff} = 0.4$ is due to the retarding of the first stage ignition, discussed in Figure 5.

The last part of this analysis focuses on NOx emissions. Figure 8 displays the variation of NOx emissions, on a basis of ppm units and maximum in-cylinder temperature, as a function of H_2O_2 addition at engine speeds of 750 (a,c) and 1150 (b,d) rpm and at $\varphi_{eff} = 0.2, 0.3$, and 0.4. NO_x emissions at φ_{eff} 0.2 and 0.3 are sufficiently low for both 750 and 1150 engine speeds. Firstly, it is shown that hydrogen peroxide addition leads to an increase of both T_{max} and NOx. The response of both T_{max} and NOx to the hydrogen peroxide addition is strongly linear for all cases considered, with the only exception the cases of sufficiently low hydrogen peroxide addition percentages. The latter
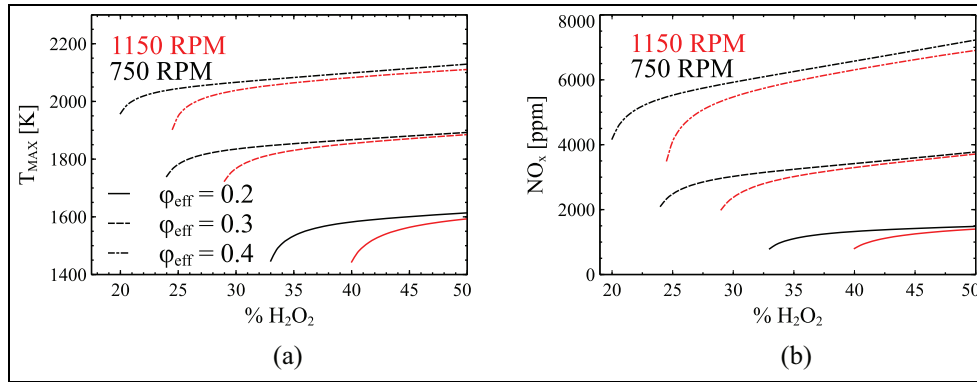
Figure 8. Variation of exhaust NO_x emissions (a) and maximum temperature (b) as a function of H_2O_2 addition for three different cases of φ_{eff} = 0.2, 0.3, 0.4 (solid, dashed, and dot dashed lines) and two different engine speeds 750 (black font) and 1150 rpm (red font).

were excluded from a linear regression analysis that aimed to determine the conditions which favor the increase of NOx and T_{max}. In all examined cases in the regression analysis, R^2 was equal to or larger than 0.95. The gradient of the best-fit line for T_{max} at 750 rpm was determined to be 355.3, 298.2 and 350.6 for φ_{eff} = 0.2, 0.3, and 0.4, respectively. These values indicate no clear trend, however, when the engine speed increases to 1150 rpm, they become 760.4, 405.5, and 396.7, for φ_{eff} = 0.2, 0.3, and 0.4, respectively. Hence, at the higher engine speed the gradient of the best-fit line decreases with the increase of φ_{eff}. Also, it must be noted that for the same φ_{eff}, the gradient increases with the engine speed. The former finding holds true for the gradient of the best-fit line for NOx as well, that is, the gradient increases with the increase of φ_{eff}: at 750 rpm, the gradient becomes 1768.7, 3816.0 and 6957.9 for φ_{eff} = 0.2, 0.3, and 0.4, respectively. The same applies for the case of 1150 rpm where the gradient of the best-fit line becomes 3669.8, 5010.0, and 7677.8 for φ_{eff} = 0.2, 0.3, and 0.4, respectively. These results in principle suggest that hydrogen peroxide addition leads to increase of NOx but this increase becomes more pronounced as φ_{eff} and/or the engine speed increase. In overall, the obtained NOx values are considered high, thereby suggesting that the proposed technology of hydrogen peroxide should most probably require some treatment for the excessive production of NOx emissions. For instance, Khalil et al.[50] reported that steam dilution may be an effective strategy for reducing significantly NOx emissions.

The effect of the incremental increase of the initial amount of hydrogen peroxide on the engine performance characteristics at constant engine load conditions

The next part of analysis considers the effect of H_2O_2 addition on NOx emissions, CAD50 and thermal efficiency whilst keeping the engine load (IMEP, indicated power, and torque) constant across an φ_{eff} range of 0.3–0.5. Essentially, the effect of increasing the φ_{eff}

incrementally in steps of 0.02 whilst also adjusting the H2O2 content to keep the engine load fixed was studied under engine speeds of 750 and 1150 rpm. This numerical campaign was performed at an engine load where torque was maintained at 62.1 N· m.

In Figure 9 we firstly observe that the required amount of hydrogen peroxide addition to achieve the desired load outcome reaches 100% when the mixture becomes very lean (φ_{eff} = 0.3), at both engine speeds. This finding indicates that from a practical point-of-view medium load conditions would only be achieved with sufficiently rich mixtures where φ_{eff} ⩾ 0.4 and hydrogen peroxide does not exceed 40%. Interestingly, the engine speed has negligible effect on the response of φ_{eff} against the hydrogen peroxide addition percentage. Note, however, that as the φ_{eff} decreases the required hydrogen peroxide addition exhibits qualitatively different response. At sufficiently rich conditions (φ_{eff} ⩾ 0.4) a small decrease of φ_{eff} would require a small decrease of the required H_2O_2 addition but as the mixture becomes very lean (φ_{eff} < 0.4) this situation changes drastically and a small decrease of the φ_{eff} would require a large increase of the hydrogen peroxide addition to maintain the same load. The threshold of φ_{eff} = 0.4 is actually associated with the change in the response of the thermal efficiency. The maximum thermal efficiency at 750 rpm (66.2%) is reached at φ_{eff} = 0.4 while at 1150 rpm the maximum n_{th} (65.6%) is obtained at φ_{eff} = 0.38. For lower φ_{eff} values the thermal efficiency drops with the increase of the hydrogen peroxide addition while for larger φ_{eff} values the opposite trend is observed. The reason for this qualitatively different response of n_{th} can be understood if we analyze the response of CAD50 (Figure 9(b)). Starting from φ_{eff} = 0.5, by decreasing the φ_{eff} while also increasing the hydrogen peroxide percentage leads to the advancement of CAD50, which is much more drastic for relatively richer conditions (φ_{eff} ⩾ 0.4). At the same time, CAD10 (indicative of the first stage ignition) is retarded, as has already been discussed. At 750 rpm and φ_{eff} = 0.4 (0.38 at 1150 rpm) CAD50 obtains the closest value to the TDC, 1.5 CAD aTDC (4.7 CAD
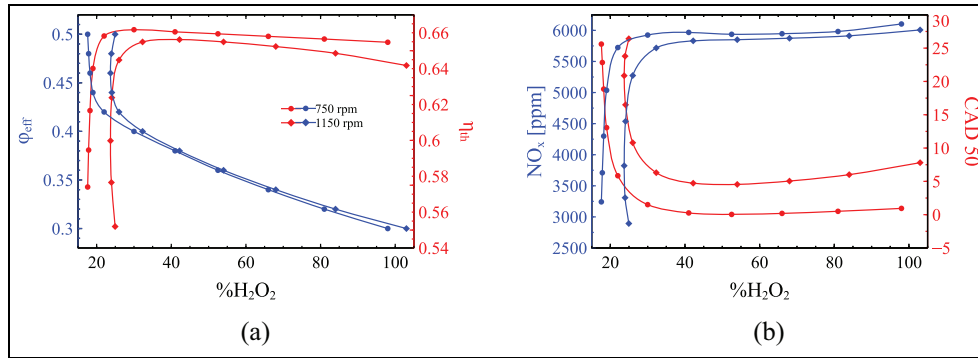
Figure 9. The effect of H₂O₂ addition on the thermal efficiency, the NOₓ emissions and CAD50 as the effective equivalence ratio is incrementally increased whilst adjusting the H₂O₂ addition to maintain constant the load at 62.1 Nm. In the following cases the effective equivalence ratio is incrementally increased from 0.3 up to 0.5 in steps of 0.02.

aTDC). However, at these limiting conditions CAD10 changes sign, that is, turning from negative (i.e. bTDC) to positive (aTDC). By decreasing further φ_{eff} while also increasing the hydrogen peroxide addition percentage leads to the further retarding of CAD10, which has an adverse effect on CAD50 (and hence the ignition process), incurring its retarding as well. Finally, reaching high thermal efficiency comes with the caveat of high NOx emissions. Generally, the increase of the hydrogen peroxide addition induces an increase in NOx emissions. This increase becomes more pronounced as CAD50 is advanced close to the TDC through the addition of hydrogen peroxide and reaches a value which is maintained largely unchanged with further increase of the hydrogen peroxide.

In the last part of the analysis, the aim was to highlight the benefits of H₂O₂ addition on the engine performance characteristics whilst providing a direct comparison with the conventional method of preheating ammonia, but opposite to the analysis so far, now heat losses are considered. The heat losses are the cause for some notable differences in the results compared to the respective ones reported in Figures 5 to 8 for the adiabatic cases. Initially, H₂O₂ was incrementally added on a mole fraction basis of NH3 in steps of 1% from 27% to 35%. The load output obtained from this exercise was then reproduced by removing the hydrogen peroxide and increasing properly the inlet temperature. If an increase in temperature did not suffice that is, the same power was not achieved using the glow-plug approach as for the case containing H₂O₂, the φ_{eff} was incrementally increased, until sufficient performance (identical to that of a respective case containing H₂O₂) was achieved. This approach was taken for each % addition of H₂O₂ from 27% to 35%. Ultimately, the overall aim was to highlight the changes in the glow plug approach required to achieve the same load in the case as with the use of hydrogen peroxide, and what these changes would entail in terms of performance, NOx and combustion phasing.

The results concerning this analysis are shown in Table 4. Firstly, the glow plug approach generally requires that the equivalence ratio is doubled and the inlet temperature is increased by more than 50% for all examined cases, while with the hydrogen peroxide approach the effective equivalence ratio and the inlet temperature are both kept fixed at 0.3 and 320 K, respectively. With regard to combustion phasing, CAD10 is consistently maintained to negative values for the hydrogen peroxide approach while in the glow plug approach it is maintained at ~11 CAD aTDC. The difference of the CAD10 values between the two approaches is in the neighborhood of 12 degrees for all cases under consideration. On the other hand, the difference in the CAD50 values between the two approaches becomes more pronounced ranging between 17 and 28 degrees. This occurs because the increase of the hydrogen peroxide addition leads to the gradual advancement of CAD50 and at the same time the increase of the equivalence ratio to reach the desired load outcome in the glow plug approach leads to the gradual retarding of CAD50. This phenomenon also explains why the difference in the RBA values between the two approaches increases gradually with the increase in the hydrogen peroxide addition. In addition, unlike to what was reported earlier in the discussion on Table 3, the difference in the thermal efficiency between the two approaches becomes more notable. The thermal efficiency with the hydrogen peroxide addition approach varies in the range of 48%–53%, which is consistently higher than the respective thermal efficiency with the glow plug approach, by 3%–7%, depending the conditions. This is a reasonable finding since most of the heat release in the hydrogen peroxide addition approach occurs close to the TDC, much closer compared to the glow plug approach. More spectacular though is the difference of the maximum reached temperature. The glow plug approach leads consistently to much higher maximum temperatures, with this difference ranging between 28% and 52% against the hydrogen peroxide addition approach. The

Table 4. Engine performance results for an engine speed of 750 rpm and an effective equivalence ratio of φ_{eff} = 0.3 with and without H_2O_2 content. Each case of $NH_3 + H_2O_2$ has a respective case of pure ammonia which is preheated. All cases with H_2O_2 content have a constant intake temperature of 320 K. Power is maintained equivalent to that achieved by incremental addition of H_2O_2, whilst using preheated ammonia and considering heat losses.

φ_{eff}	%H_2O_2	T_{in} (K)	CAD10 (CAD aTDC)	CAD50 (CAD aTDC)	RBA	Torque (Nm)	n_{th}	T_{max} (K)	NOx (ppm)	P_{max} (bar)
0.30	27.00	320.0	−1.69	7.79	18.20	37	52.54	1585.52	1154.82	72.23
0.66	0	493.2	10.99	25.23	14.43	37	45.61	2416.84	10,021.95	47.36
0.30	28.00	320.0	−1.71	5.56	10.93	36	51.47	1718.12	1976.51	89.21
0.64	0	492.0	10.71	24.29	13.70	36	45.93	2397.16	9995.15	48.49
0.30	29.00	320.0	−1.72	4.16	8.54	36	50.69	1753.12	2267.99	96.31
0.64	0	491.9	10.80	27.14	16.53	36	45.45	2357.48	9450.58	45.60
0.30	30.00	320.0	−1.72	3.15	7.08	36	50.10	1772.91	2448.56	100.10
0.62	0	490.8	10.42	23.63	13.33	36	46.24	2377.78	9934.24	49.77
0.30	31.00	320.0	−1.72	2.38	6.04	36	49.62	1786.60	2580.32	102.50
0.62	0	490.7	10.49	25.11	14.78	36	46.00	2352.87	9572.25	45.89
0.30	32.00	320.0	−1.73	1.77	5.26	35	49.24	1797.00	2684.29	104.15
0.62	0	490.7	10.49	25.24	14.92	35	45.84	2340.96	9396.48	45.73
0.30	33.00	320.0	−1.72	1.27	4.62	35	48.91	1805.43	2771.33	105.36
0.62	0	490.7	10.53	26.56	16.25	35	45.74	2331.96	9262.62	45.73
0.30	34.00	320.0	−1.72	0.87	4.12	35	48.36	1812.40	2845.39	106.26
0.62	0	490.7	10.55	27.27	16.97	35	45.68	2327.25	9192.38	45.73
0.30	35.00	320.0	−1.71	0.54	3.68	35	48.39	1818.53	2912.20	106.99
0.62	0	490.7	10.55	27.27	16.96	35	45.66	2326.98	9188.42	45.73

higher maximum temperatures reached in the glow plug approach are the result of the higher employed equivalence ratios and inlet temperatures. These higher temperatures directly affect the production of NOx emissions which increase by a factor of 3 to a factor of 9 (almost an order of magnitude) compared to the hydrogen peroxide addition approach. Finally, in agreement with what was reported earlier in the discussion on Table 3, the only caveat with the use of hydrogen peroxide is the increased maximum pressures, which when compared to the glow plug approach exhibit increases which range between 50% and 130%.

Conclusions

Ammonia is one of few main candidates for future use in heavy duty applications, however its unrealistic ignition delay times due to its high auto-ignition temperature has made it an unattractive solution for the decarbonization of heavy duty applications. In the current study, hydrogen peroxide was considered as an ignition promoter of an ammonia-fulled HCCI engine. The numerical work was conducted on the basis of a single zone simplified model available in the Chemkin Pro suite, using a detailed chemical kinetic model.[54] The objective of the work was to provide numerical evidence for the feasibility of the proposed technology, while also identifying potential challenges in its implementation. The employed numerical model, albeit simplified, enabled the qualitative analysis of the proposed technology and the identification of trends that will inform future experiments and/or computationally expensive high fidelity numerical simulations. The employed numerical model despite its inherent weaknesses provided valuable insight about the feasibility of the new technology, yet the produced results and the

reached conclusions should be interpreted with care, due to lack of proper validation with engine experiments.

The conclusions can be summarized as follows:

- hydrogen peroxide addition was proven to be advantageous against the more conventional approach of preheating the ammonia/air charge, typically done with the use of a glow plug. In particular, the hydrogen peroxide addition led to significantly higher IMEP, power and torque, mainly due to the increase of the mixture's energy density. The thermal efficiency exhibited much lower, yet non-negligible, increase. NOx emissions were also found to decrease tremendously. Under constant load conditions, the hydrogen peroxide addition approach led to a 9-fold decrease in NOx. Yet the obtained NOx emission values were still high, thereby suggesting the necessity for the use of an additional technology for their treatment.
- the introduction of hydrogen peroxide leads to a two-stage ignition process. The first ignition stage is instrumental in the control of the whole ignition process since it was found to be retarded with the increase of the hydrogen peroxide addition while the second ignition stage was advanced. This led to: (i) a rapid decrease of the RBA and (ii) a non-monotonic response of the ignition CAD to the hydrogen peroxide addition.
- hydrogen peroxide addition generally leads to higher IMEP, power, torque, and NOx emissions values. In fact these variables largely exhibit linear response to the hydrogen peroxide addition. Linear regression analysis revealed that hydrogen peroxide tends to increase IMEP, power and torque and this tendency is favored as the effective equivalence ratio increases. As the engine speed increases the

response of IMEP, power and torque are characterized by a higher rate of change but this phenomenon becomes attenuated as the effective equivalence ratio increases. Additionally, hydrogen peroxide addition leads to increase of NOx but this increase becomes more pronounced as the effective equivalence ratio and/or the engine speed increase.

- the incremental addition of hydrogen peroxide leads initially to a rapid increase of the thermal efficiency which at some point reaches a maximum value and after that point further increase of the hydrogen peroxide addition leads to a gradual decrease of the thermal efficiency. The thermal efficiency is achieved when CAD50 gets closest to the TDC. As the mixture becomes leaner the CAD50 associated with the maximum thermal efficiency is advanced and in the case of sufficiently lean coditions it even becomes negative.

The results presented herein for the feasibility of the proposed use of hydrogen peroxide as an ignition promoter for ammonia use in CI engines, are promising. Yet, further research is required. Few of the issues that we believe merit further investigation, as highlighted by the current works, are:

- the chemical mechanism that is responsible for the control of the two ignition stages, particularly the first stage ignition which was found to be key to the control of the ignition process;
- the implementation of different strategies for NOx mitigation such as the use of exhaust gas recirculation (EGR) or steam dilution;
- the limitations in terms of the pressure rise rate and the combustion efficiency.

Declaration of conflicting interests

Funding

ORCID iDs

Omar Shafiq https://orcid.org/0000-0003-2577-243X
Efstathios-Al. Tingas https://orcid.org/0000-0001-8849-1251

References

1. European Environment Agency. EEA greenhouse gases-data viewer. https://www.eea.europa.eu/data-and-maps/data/data-viewers/greenhouse-gases-viewer (2021, accessed 21 March 2021).

2. Conway G, Joshi A, Leach F, García A and Senecal PK. A review of current and future powertrain technologies and trends in 2020. *Transp Eng* 2021; 5: 100080.

3. Grantham Research Institute on Climate Change and the Environment. Climate Change Laws of the World, https://climate-laws.org/ (accessed 5 June 2022).

4. Logan KG, Hastings A and Nelson JD. *Introduction.* Cham: Springer International Publishing, 2022, pp.1–17.

5. HM Government. Net zero strategy: build back greener, https://assets.publishing.service.gov.uk/government/uploads/system/uploads/attachment data/file/1033990/net-zero-strategy-beis.pdf (October 2021).

6. Norwegian Government. Climate Action Plan, https://www.regjeringen.no/contentassets/ 202fec60ac844d4ca7d53d65b6b9ac9c/ alle-regjeringa-vil-punkt-i-meldinga.pdf (January 2021).

7. Regeringskansliet. Klimatpolitiska handlingsplanen (Climate Policy Action Plan), https://www.regeringen.se/4af76e/contentassets/fe520eab3a954eb39084aced9490b14c/klimatpolitiska-handlingsplanen-fakta-pm.pdf (December 2019).

8. Government of the Netherlands, Climate Act, Staatsblad van het Koninkrijk der Nederlanden, January 2019.

9. Zeng X, Li M, Abd El-Hady D, et al. Commercialization of lithium battery technologies for electric vehicles. *Adv Energy Mater* 2019; 9(27): 1900161.

10. Schmuch R, Wagner R, Hörpel G, Placke T and Winter M. Performance and cost of materials for lithium-based rechargeable automotive batteries. *Nat Energy* 2018; 3(4): 267–278.

11. Gunawan TA and Monaghan RFD. Techno-econo-environmental comparisons of zero- and low-emission heavy-duty trucks. *Appl Energy* 2022; 308: 118327.

12. Panoutsou C, Germer S, Karka P, et al. Advanced biofuels to decarbonise European transport by 2030: markets, challenges, and policies that impact their successful market uptake. *Energy Strategy Rev* 2021; 34: 100633.

13. Chiong MC, Chong CT, Ng JH, et al. Advancements of combustion technologies in the ammonia-fuelled engines. *Energy Convers Manag* 2021; 244: 114460.

14. Valera-Medina A, Xiao H, Owen-Jones M, David WI and Bowen PJ. Ammonia for power. *Prog Energy Combust Sci* 2018; 69: 63–102.

15. MacFarlane DR, Cherepanov PV, Choi J, et al. A roadmap to the ammonia economy. *Joule* 2020; 4(6): 1186–1205.

16. Cardoso JS, Silva V, Rocha RC, Hall MJ, Costa M and Eusébio D. Ammonia as an energy vector: current and future prospects for low-carbon fuel applications in internal combustion engines. *J Clean Prod* 2021; 296: 126562.

17. Dimitriou P and Javaid R. A review of ammonia as a compression ignition engine fuel. *Int J Hydrogen Energy* 2020; 45(11): 7098–7118.

18. Cornelius W, Huellmantel LW and Mitchell HR. Ammonia as an engine fuel. *SAE Transactions* 1966; 74: 300–326.

19. Ashirbad A and Agarwal AK. Scope and limitations of ammonia as transport fuel. In: AK Agarwal, H Valera (eds) *Greener and scalable E-fuels for decarbonization of transport.* Springer, 2022, pp.391–418. https://link.springer.com/book/10.1007/978-981-16-8344-2

20. Mounaïm-Rousselle C and Brequigny P. Ammonia as fuel for low-carbon spark-ignition engines of tomorrow's passenger cars. *Front Mech Eng* 2020; 6: 70.

21. Lhuillier C, Brequigny P, Contino F and Mounaïm-Rousselle C. Experimental investigation on ammonia

combustion behavior in a spark-ignition engine by means of laminar and turbulent expanding flames. *Proc Combust Inst* 2021; 38(4): 5859–5868.

22. Lhuillier C, Brequigny P, Contino F and Mounaïm-Rousselle C. Experimental study on ammonia/hydrogen/air combustion in spark ignition engine conditions. *Fuel* 2020; 269: 117448.

23. Comotti M and Frigo S. Hydrogen generation system for ammonia–hydrogen fuelled internal combustion engines. *Int J Hydrogen Energy* 2015; 40(33): 10673–10686.

24. Frigo S and Gentili R. Analysis of the behaviour of a 4-stroke SI engine fuelled with ammonia and hydrogen. *Int J Hydrogen Energy* 2013; 38(3): 1607–1615.

25. Kurien C and Mittal M. Review on the production and utilization of green ammonia as an alternate fuel in dual-fuel compression ignition engines. *Energy Convers Manag* 2022; 251: 114990.

26. Van Blarigan P. Advanced internal combustion engine research. *DOE Hydrogen Program Review NREL-CP-570-28890*, 2000, pp.1–19.

27. Gray JT Jr, Dimitroff E, Meckel NT, et al. Ammonia fuel—engine compatibility and combustion. *SAE Transactions* 1967; 75 785–807.

28. Pochet M, Truedsson I, Foucher F, et al. Ammonia-hydrogen blends in homogeneous-charge compression-ignition engine. SAE technical papers 2017-24-0087, 2017.

29. Reiter AJ and Kong SC. Combustion and emissions characteristics of compression-ignition engine using dual ammonia-diesel fuel. *Fuel* 2011; 90(1): 87–97.

30. Reiter AJ and Kong SC. Diesel engine operation using ammonia as a carbon-free fuel. In *Internal combustion engine division fall technical conference*, volume 49446. ASME. pp.111–117.

31. Gross CW and Kong SC. Performance characteristics of a compression-ignition engine using direct-injection ammonia–DME mixtures. *Fuel* 2013; 103: 1069–1079.

32. Ryu K, Zacharakis-Jutz GE and Kong SC. Performance characteristics of compression-ignition engine using high concentration of ammonia mixed with dimethyl ether. *Appl Energy* 2014; 113: 488–499.

33. Tay KL, Yang W, Li J, et al. Numerical investigation on the combustion and emissions of a kerosene-diesel fueled compression ignition engine assisted by ammonia fumigation. *Appl Energy* 2017; 204: 1476–1488.

34. Tay KL, Yang W, Chou SK, et al. Effects of injection timing and pilot fuel on the combustion of a kerosene-diesel/ammonia dual fuel engine: a numerical study. *Energy Proc* 2017; 105: 4621–4626.

35. Wang Y, Zhou X and Liu L. Theoretical investigation of the combustion performance of ammonia/hydrogen mixtures on a marine diesel engine. *Int J Hydrogen Energy* 2021; 46(27): 14805–14812.

36. Ezzat MF and Dincer I. Development and assessment of a new hybrid vehicle with ammonia and hydrogen. *Appl Energy* 2018; 219: 226–239.

37. Wernimont E, Ventura M, Garboden G, et al. Past and present uses of rocket grade hydrogen peroxide. *General Kinetics* 1999; 92656.

38. Yeom JK, Jung SH and Yoon JH. An experimental study on the application of oxygenated fuel to diesel engines. *Fuel* 2019; 248: 262–277.

39. Fanz B and Roth P. Injection of a H2O2/water solution into the combustion chamber of a direct injection diesel engine and its effect on soot removal. *Proc Combust Inst* 2000; 28(1): 1219–1225.

40. Krishna BM. Experimental investigation on CI engine with hydrogen peroxide as an alternate. *Glob J Res Eng* 2020; 20(1): 37–41.

41. Trapel E, Ifeacho P and Roth P. Injection of hydrogen peroxide into the combustion chamber of diesel engine: effects on the exhaust gas behaviour. SAE technical paper 2004-01-2925, 2004.

42. Nguyen KB, Dan T and Asano I. Combustion, performance and emission characteristics of direct injection diesel engine fueled by jatropha hydrogen peroxide emulsion. *Energy* 2014; 74: 301–308.

43. Zhou A, Zhang C, Li Y, Li S and Yin P. Effect of hydrogen peroxide additive on the combustion and emission characteristics of an n-butanol homogeneous charge compression ignition engine. *Energy* 2019; 169: 572–579.

44. Dimitrova ID, Megaritis T, Ganippa LC and Tingas EA. Computational analysis of an hcci engine fuelled with hydrogen/hydrogen peroxide blends. *Int J Hydrogen Energy* 2022; 47(17): 10083–10096.

45. Tingas EA. Computational analysis of the effect of hydrogen peroxide addition on premixed laminar hydrogen/air flames. *Fuel* 2021; 302: 121081.

46. Tingas EA. The chemical dynamics of hydrogen/hydrogen peroxide blends diluted with steam at compression ignition relevant conditions. *Fuel* 2021; 296: 120594.

47. Fukuzumi S, Yamada Y and Karlin KD. Hydrogen peroxide as a sustainable energy carrier: electrocatalytic production of hydrogen peroxide and the fuel cell. *Electrochim Acta* 2012; 82: 493–511.

48. Khalil AT, Manias DM, Tingas EA, Kyritsis DC and Goussis DA. Algorithmic analysis of chemical dynamics of the autoignition of NH3–H2O2/air mixtures. *Energies* 2019; 12(23): 4422.

49. Wu FH and Chen GB. Numerical study of hydrogen peroxide enhancement of ammonia premixed flames. *Energy* 2020; 209: 118118.

50. Khalil AT, Manias DM, Kyritsis DC and Goussis DA. No formation and autoignition dynamics during combustion of H2O-diluted NH3/H2O2 mixtures with air. *Energies* 2020; 14(1): 84.

51. Yang W, Al Khateeb AN and Kyritsis DC. The effect of hydrogen peroxide on NH3/O2 counterflow diffusion flames. *Energies* 2022; 15(6): 2216.

52. Chemkin-Pro A. 21.0. ANSYS reaction design: San Diego, 2021.

53. Zhang C and Wu H. The simulation based on CHEMKIN for homogeneous charge compression ignition combustion with on-board fuel reformation in the chamber. *Int J Hydrogen Energy* 2012; 37(5): 4467–4475.

54. Zhang Z, Xie Q, Liang J and Li G. Numerical study of combustion characteristics of a natural gas HCCI engine with closed loop exhaust-gas fuel reforming. *Appl Therm Eng* 2017; 119: 430–437.

55. Yao M, Zheng Z and Liu H. Progress and recent trends in homogeneous charge compression ignition (HCCI) engines. *Prog Energy Combust Sci* 2009; 35(5): 398–437.

56. Aroonsrisopon T, Werner P, Waldman JO, et al. Expanding the HCCI operation with the charge stratification. *SAE transactions* 2004; 1130–1145.

57. Dec JE, Yang Y and Dronniou N. Boosted HCCI - controlling pressure-rise rates for performance improvements using partial fuel stratification with conventional gasoline. *SAE Int J Engines* 2011; 4(1): 1169–1189.

58. Yang Y, Dec JE, Dronniou N and Sjöberg M. Tailoring HCCI heat-release rates with partial fuel stratification: comparison of two-stage and single-stage-ignition fuels. *Proc Combust Inst* 2011; 33(2): 3047–3055.

59. Zhang X, Moosakutty SP, Rajan RP, Younes M and Sarathy SM. Combustion chemistry of ammonia/hydrogen mixtures: jet-stirred reactor measurements and comprehensive kinetic modeling. *Combust Flame* 2021; 234: 111653.

60. Bendu H and Murugan S. Homogeneous charge compression ignition (HCCI) combustion: mixture preparation and control strategies in diesel engines. *Renew Sustain Energ Rev* 2014; 38: 732–746.

61. Singh AP and Agarwal AK. Combustion characteristics of diesel HCCI engine: an experimental investigation using external mixture formation technique. *Appl Energy* 2012; 99: 116–125.

62. Hairuddin AA, Yusaf T and Wandel AP. A review of hydrogen and natural gas addition in diesel HCCI engines. *Renew Sustain Energ Rev* 2014; 32: 739–761.

63. Hui X, Zheng D, Zhang C, Xue X and Sung CJ. Effects of hydrogen peroxide addition on two-stage ignition characteristics of n-heptane/air mixtures. *Int J Hydrogen Energy* 2019; 44(44): 24312–24320.

64. Fukuzumi S and Yamada Y. Hydrogen peroxide used as a solar fuel in one-compartment fuel cells. *ChemElectroChem* 2016; 3(12): 1978–1989.

65. Kobayashi H, Hayakawa A, Somarathne KD and Okafor E. Science and technology of ammonia combustion. *Proc Combust Inst* 2019; 37(1): 109–133.

66. Mathieu O and Petersen EL. Experimental and modeling study on the high-temperature oxidation of ammonia and related NOx chemistry. *Combust Flame* 2015; 162(3): 554–570.

67. Xiao H, Lai S, Valera-Medina A, Li J, Liu J and Fu H. Experimental and modeling study on ignition delay of ammonia/methane fuels. *Int J Energy Res* 2020; 44(8): 6939–6949.

68. He X, Shu B, Nascimento D, Moshammer K, Costa M and Fernandes RX. Auto-ignition kinetics of ammonia and ammonia/hydrogen mixtures at intermediate temperatures and high pressures. *Combust Flame* 2019; 206: 189–200.

Appendix

Abbreviations

aTDC	After Top Dear Center
bTDC	Before Top Dead Center
CAD	Crank Angle Degrees
CAD10	The Crank Angle Degrees at 10% Heat Release
CAD50	The Crank Angle Degrees at 50% Heat Release
CAD90	The Crank Angle Degrees at 90% Heat Release
CI	Compression Ignition
CSP	Computational Singular Perturbation
DME	Dimethyl-ether
EGR	Exhaust Gas Recirculation
HCCI	Homogeneous Charge Compression Ignition
IMEP	Indicated Mean Effective Pressure
RBA	Rapid Burning Angle
RPM	Rounds Per Minute
SI	Spark Ignition
TDC	Top Dead Center